www.czasopisma.pan.pl PAN POLSKA AKADEMIA NAUK www.journals.pan.pl

PAN ARCHIVES OF ACOUSTICS
Vol. 40, No. 2, pp. 151–157 (2015)

DOI: 10.1515/aoa-2015-0017

Research Papers

A Simulation for Detecting Nonlinear Echoes from Microbubbles Packets

Mohamed G.S. ALI, Nour Z. ELSAYED, Ebtsam A. EID

Physics Department, Faculty of Science, Minia University
Egypt; e-mail: Mgalal09@yahoo.com

(*received March 19, 2014; accepted July 24, 2014*)

This work presents a simulation of the response of packets of microbubbles in an ultrasonic pulse-echo scan line. Rayleigh-Plesset equation has been used to predict the echo from numerically obtained radial dynamics of microbubbles. Varying the number of scattering microbubbles on the pulse wave form has been discussed. To improve microbubble-specific imaging at high frequencies, the subharmonic and second harmonic signals from individual microbubbles as well as microbubbles packets were simulated as a function of size and pressure. Two different modes of harmonic generation have been distinguished. The strength and bandwidth of the subharmonic component in the scattering spectrum of microbubbles is greater than that of the second harmonic. The pressure spectra provide quantitative and detailed information on the dynamic behaviour of ultrasound contrast agent microbubbles packet.

Keywords: microbubbles packets, harmonic component, acoustic, radial dynamic, pressure spectrum.

1. Introduction

The dynamics of a single gas bubble in free space was first described by (Rayleigh, 1917) and was later refined (Plesset, 1947; Neppiras, Noltingk, 1951; Noltingk, Neppiras, 1950; Poritsky, 1952) to account for surface tension and viscosity of the liquid. There are a large number of investigations on the radial motion of the bubble (Prosperetti, 1984; Feng, Leal, 1997). If a bubble experiences a time-varying pressure field (such as an incoming ultrasound wave) it will react with compression or expansion. Depending on the amplitude of the ultrasound wave, the vibrations will be related either linearly or nonlinearly to the applied acoustic pressure. For low acoustic pressures, the instantaneous radius oscillates linearly in relation to the amplitude of the applied external pressure field. For higher amplitudes of the external field, the pulsation of the bubbles becomes nonlinear. The deformation of two bubbles' surfaces was investigated by (Liang *et al.*, 2012) and the area of stability about initial radius and sound pressure for two interacting bubbles was obtained. Sijl *et al.* (2011b) showed that the radial dynamics of an isolated oscillating microbubble can be used to predict its acoustic emission.

In this paper we present a simulation of the signal pathway in a simple pulse-echo system operating in a fluid which contains number of microbubbles. This simulation enables us to study the effect of scattering pressure on pulse waveforms, and how it affects the spatial resolution of the system. Microbubbles are excited by the transmitted pulse into an oscillation, which in turn converts into an acoustic response received by the ultrasound system. This path is schematically presented in Fig. 1. It is clear that the response

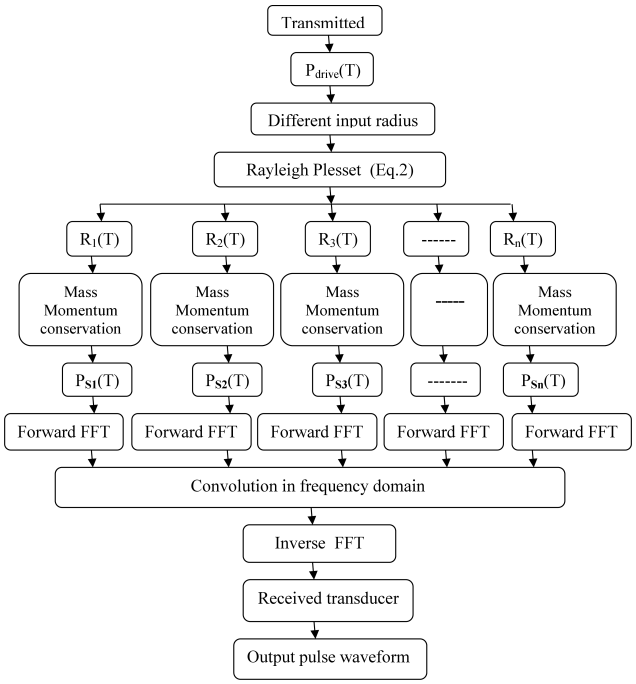

Fig. 1. Function block diagram of system model.

from packets of microbubbles is predicted. The simulation of the signal path includes the microbubbles response and the electro-acoustic properties of the transducer. The approach taken is to assume that these two processes are time invariant and separable from each other. The overall signal pathway is assumed to be the convolution of two impulse response representing the transducer and microbubbles respectively. Equivalently, the signal pathway can be considered in the frequency domain as a multiplication of the transfer function representing each of the two phenomena.

2. Theory

If the bubble is considered spherical and is surrounded by an incompressible liquid of infinite extent the kinetic energy supplied to the surrounding liquid should balance the difference between the work performed by the fluid far from the bubble and that at the bubble wall and the Rayleigh-Plesset equation is obtained

$$\rho\left(R\ddot{R}+3\frac{\dot{R}^2}{2}\right)=(P_L-P_\infty). \tag{1}$$

In this equation R, $\dot{R}$, and $\ddot{R}$ describe the radius, the velocity and the acceleration of the bubble wall respectively. The pressure difference is determined by the pressure in the liquid at the bubble wall, P_L, and the pressure far from the bubble wall, P_∞. If we neglect viscosity and the vapor pressure inside the bubble and assuming that the gas inside the bubble is described by the polytropic ideal gas law $P_g \propto R^{-3\gamma}$, where γ is the polytropic exponent, the following equation can be obtained:

$$P_L=\left(P_0+\frac{2\sigma}{R_0}\right)\left(\frac{R_0}{R}\right)^{3\gamma}-\frac{2\sigma}{R}-\frac{4\mu}{R}\dot{R}. \tag{2}$$

Inserting Eq. (2) into Eq. (1) the total equation becomes:

$$\rho\left(R\ddot{R}+3\frac{\dot{R}^2}{2}\right)=\left(P_0+\frac{2\sigma}{R_0}\right)\left(\frac{R_0}{R}\right)^{3\gamma}-\frac{4\mu}{R}\dot{R}-\frac{2\sigma}{R_0}-P_0-P(t). \tag{3}$$

In this equation the initial bubble radius is given by R_0 and the ambient pressure by P_0. The driving pressure pulse is described by $P(t)$, σ the surface tension, μ the viscosity of the surrounding liquid and $P(t)$ is the applied acoustic field.

The sound emitted by an oscillating microbubble consists of two parts. The first is a passive contribution that results from the geometrical scattering of the microbubble (could also be a non-oscillating body) in the incident ultrasound field and the second is an active contribution that results from the volumetric oscillations of the bubble. In regular applications, ultrasound contrast microbubbles are much smaller than the incident wavelength and the passive contribution can be safely neglected. The active contribution is determined by the radial dynamics of the microbubble, described by the radius time curve $R(t)$. From the conservation of mass and momentum it follows that the emitted pressure wave $P_s(r,t)$, at a distance r, is determined from the second time derivative of the volume V of the bubble

$$P_s\left(r,t-r/c\right)=\frac{\rho}{4\pi r}\ddot{V}(t)=\frac{\rho}{3r}\frac{\partial^2}{\partial t^2}\left[\ddot{R}(t)^3\right], \tag{4}$$

where ρ is the density of the surrounding liquid. The finite time for the pressure wave to travel a distance r from the bubble wall to the transducer surface is accounted for by the term r/c where c is the speed of sound in the liquid medium. A regularly used form of Eq. (4) is obtained by rewriting:

$$P_s\left(r,t-r/c\right)=\frac{\rho}{r}\left[R(t)^2\ddot{R}(t)+2R(t)\dot{R}(t)^2\right]. \tag{5}$$

In the equations it is assumed that the receiver is sufficiently far from the microbubble to neglect the Bernoulli pressure (also referred to as the kinetic wave), which decreases with $1/r^4$ (Vokurka, 1985; Leighton, 1994). Furthermore, Eq. (4) accounts only for volumetric oscillations of the bubble. The Runga Kutta fourth order algorithm will be used to simulate the Eq. (3) with boundary condition $R(t=0)=R_0$ and $\dot{R}(t=0)=0.0$.

3. The transducer response

There are many computer models describing the behaviour of ultrasonic piezoelectric transducer. In this work, the simulation was carried out by using a previously developed digital computer model (Ali, 2000) to evaluate the pulse-echo responses of circular ultrasonic piezoelectric thickness expanders. The above simulation was applied using typical data for transducer constructed with a load zirconate titanate (PZT-5A) piezoelectric element with tungsten-epoxy (Ali, 1999) ($z=19\times10^6$ kg m^{-2}s^{-1}) back block. The transmitter response is obtained for a 10 mm diameter pulse-echo transducer of 5 MHz center frequency. Figure 2a shows the front face pressure output response expected waveform at the transducer terminals. Figure 2b shows the spectrum of the front face pressure output. From this, it can be seen that the pressure spectrum yield -3 dB bandwidth of 37.1% of the center frequency. Figure 2c shows the expected waveform at the transducer terminals when the device acts as a receiver for the force waveform of Fig. 2a.

a)

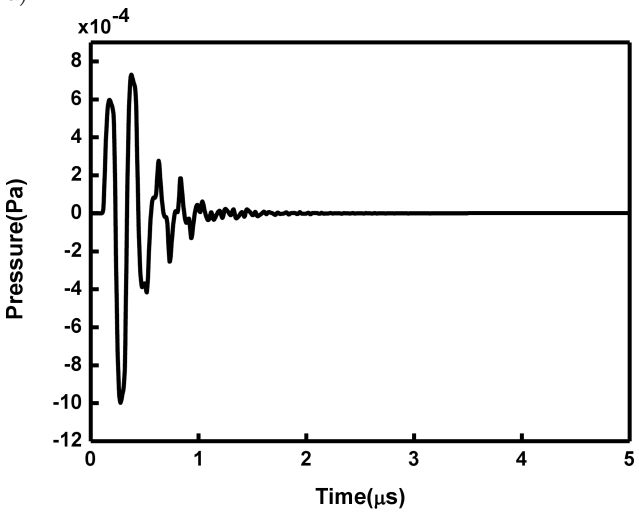

b)

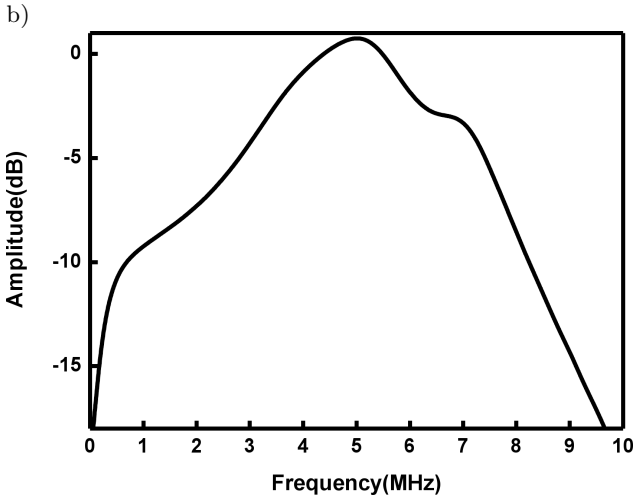

c)

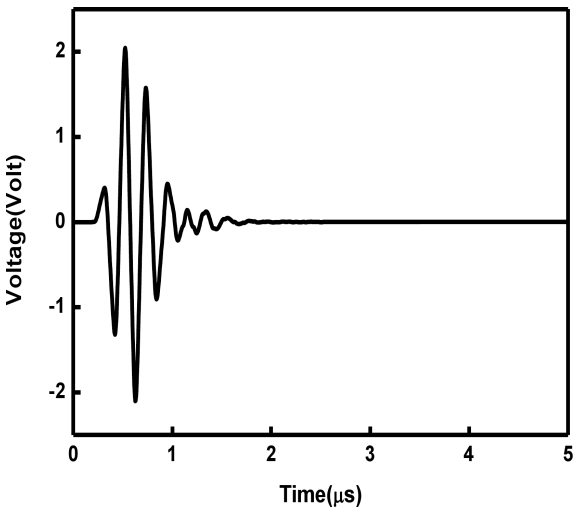

Fig. 2. Simulation of a 5 MHz pulse-echo transducer: a) the front face pressure output response, b) pulse-echo frequency response for pressure response, c) the expected waveform at the transducer terminals when the device acts as a receiver for the force waveform of Fig. 1a; that is in pulse-echo mode with no field effects.

4. Overall system response

The signal pathway of a pulse-echo system consists of the response of the transducer in transmission and reception combined with the scattered pressure response described by Eq. (4). The signal transfer process can be modelled by a series of convolution. If $x(t)$ is the input voltage drive to the pulse-echo transducer and $v(t)$ is the output voltage at the transducer terminals in reception, then

$$y(t) = f_T(t) * P_s(t) * f_R(t) * x(t), \tag{6}$$

where $*$ represents the convolution integral given by

$$g(t) * q(t) = \int_{-\infty}^{+\infty} q(\tau) g(t-\tau)\,\mathrm{d}\tau. \tag{7}$$

The symbols have the following meanings: $f_T(t)$ is transmission transducer impulse response $P_s(t)$ is scatter bubble response $f_R(t)$ is the receiver transducer impulse response.

The real frequency model is obtained from the impulse response by a Fourier transformation and replacing the time domain convolution by a frequency domain multiplication, thus

$$Y(j\omega) = F_T(j\omega) P_s(j\omega) F_r(j\omega) X(j\omega), \tag{8}$$

where

$$Y(j\omega) = \int_{-\infty}^{+\infty} y(t) e^{-j\omega t}\,\mathrm{d}t. \tag{9}$$

5. Simulation results

The simulation was carried out by multiplying the transfer functions of the two transducer responses by the transfer function of scattered pressure of microbubbles. The resulting response was then converted back into discrete time domain by inverse Fourier transformation. In order to investigate the combined effects of the transducer and the bubbles response described above on scanning system performance the simulation was applied to a medium of water containing number of bubbles. It was assumed that ultrasound contrast microbubbles are gaseous and much smaller than the incident field wavelength. The active contribution to the scattered ultrasound field was determined by the radial dynamics of the microbubble described by $R(t)$. The microbubbles were assumed to be spherical at all times. The original parameters be summarized as the liquid is water, the environmental temperature is 298 K, liquid density $\rho = 1000$ Kg/m^3, viscosity $\eta = 0.001$ Pa·s, surface tension $\sigma = 4$ Pa m, the polytropic index $\kappa = 1.4$, velocity of sound in water $c = 1480$ m/s, the static pressure $P_0 = 101.3$ KPa, and the vapor pressure $p_v = 3.2718$ KPa. The driving pressure as shown in Fig. 2a was used as input to Eq. (3) to

calculate the radial response of a 4 μm radius air microbubble in water and to calculate the scattered pulse (Eq. (4)). The pulse-echo response of the transducer shown in Fig. 2c was convolved with the scattered pulse response. The overall time domain voltage response at the receiver terminals from microbubble is shown in Fig. 3a. The frequency domain is the amplitude of the Fast Fourier transform of the overall pulse. Figure 3b shows the amplitude spectrum pulse. It is clear that the linear response is observed for small driving pulse amplitude and yield −3 dB bandwidth of 28% of the center frequency. Assuming microbubbles have different diameters independent and separable from each other. The scattered pulse for a package of microbubbles was carried out by multiplying the transfer functions for each microbubble in the frequency domain. The resulting response was then converted back into the discrete time domain by inverse Fourier transformation. Figure 4 shows the scattered pulse of five microbubbles of diameters 3, 4, 5, and 6 μm. Figure 5 shows

a)

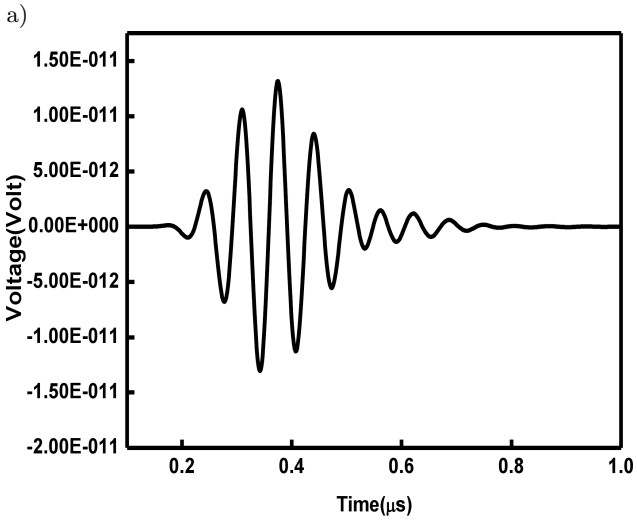

b)

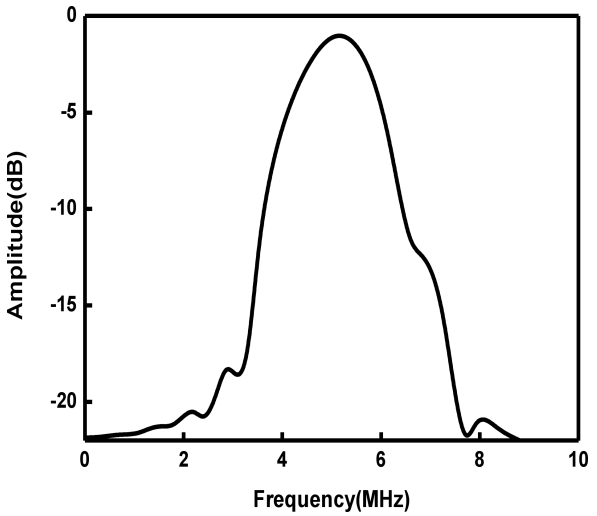

Fig. 3. a) Time domain pulse-echo response operating into 4 μm microbubble, b) pulse-echo frequency response for Fig. 3a.

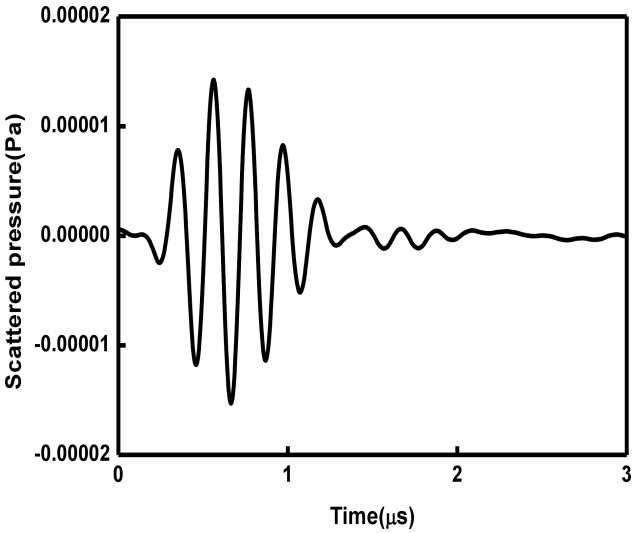

Fig. 4. Simulated scatter response of a air microbubbles package with radius 3, 4, 5, and 6 μm in water.

a)

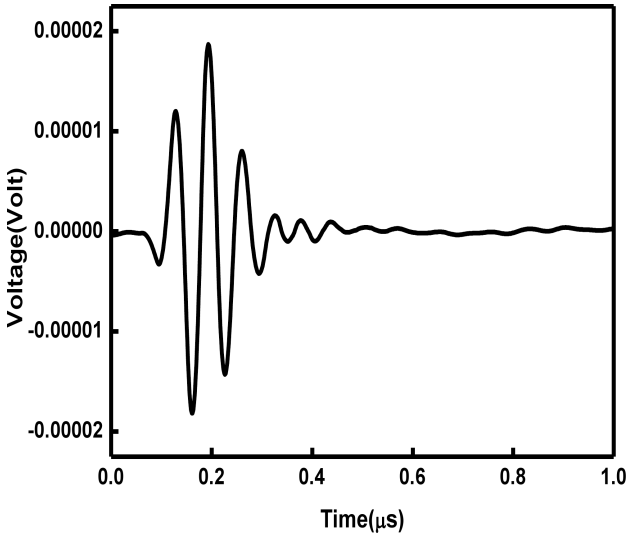

b)

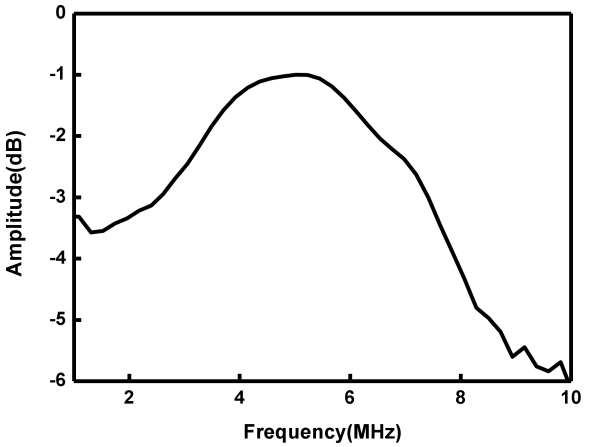

Fig. 5. Simulated pulse-echo response of a air microbubbles package with radius 3, 4, 5, and 6 μm in water: a) the voltage at the terminals when an echo is received from a microbubbles package, b) pulse-echo frequency response.

the overall voltage response and frequency response at the transducer terminal from a packet of microbubbles. It is clear from this figure that the duration of time decreased to 0.4 μs and −3 dB bandwidth yield 94% of the center frequency.

5.1. Nonlinear response

In the paragraph presented above the bubble is oscillating linearly, and no signal appears at the higher frequencies. A detailed theoretical understanding of the source of this nonlinear behavior was provided by (Sijl *et al.*, 2011a) through a weakly nonlinear analysis of the shell buckling model proposed by (Marmottant *et al.*, 2005). At higher driving frequencies a strong subharmonic component develops after a few cycles of the driving pulse (Sijl, 2010). The driving pressure function was an envelope with 5 MHz center frequency. A Hanning pulse was chosen as it is a typical medical ultrasound pulse (Fig. 6). Radius-time and pressure-time responses were simulated for microbubbles at a driving pulse of 2.0 MPa and 5 MHz.

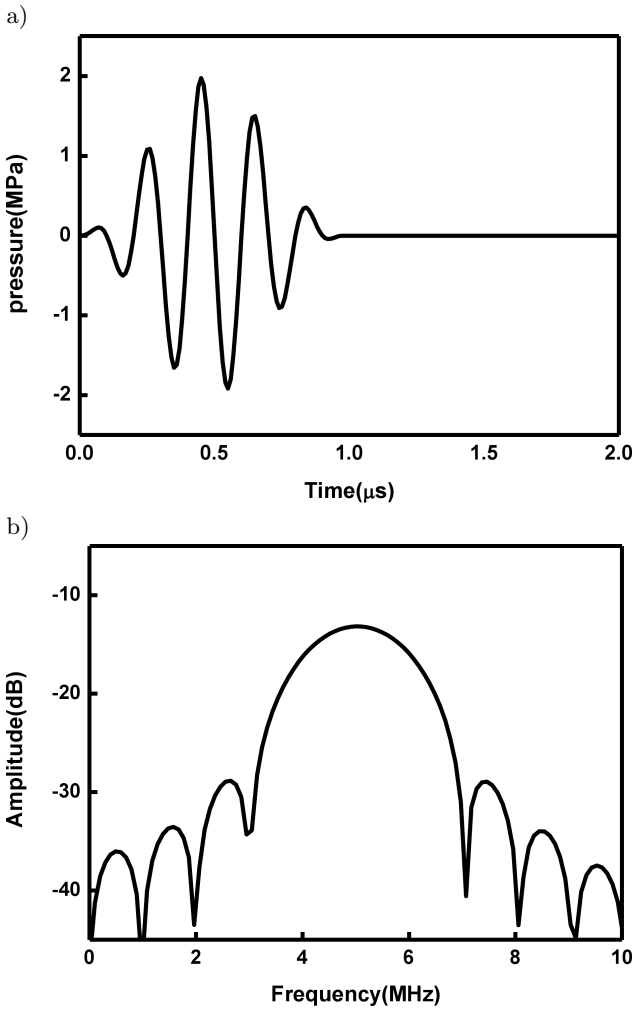

Fig. 6. a) Hanning pulse, center frequency 5 MHz, and 2 MPa amplitude, b) amplitude spectrum.

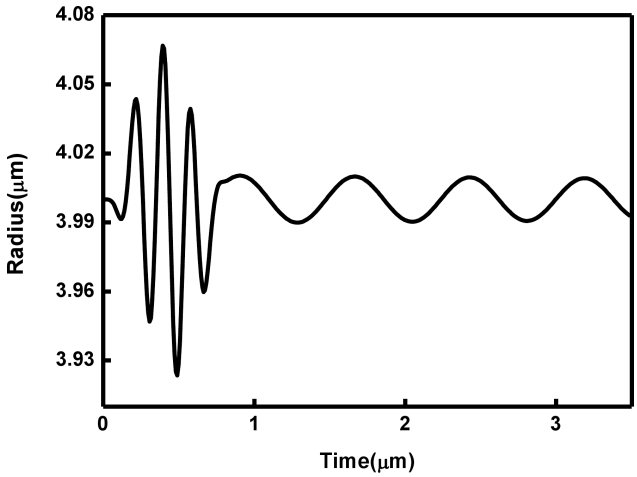

Fig. 7. The simulated radial response. The initial bubble radius was 4 μm. The driving pressure pulse had peak amplitude of 2 MPa and a frequency of 5 MHz.

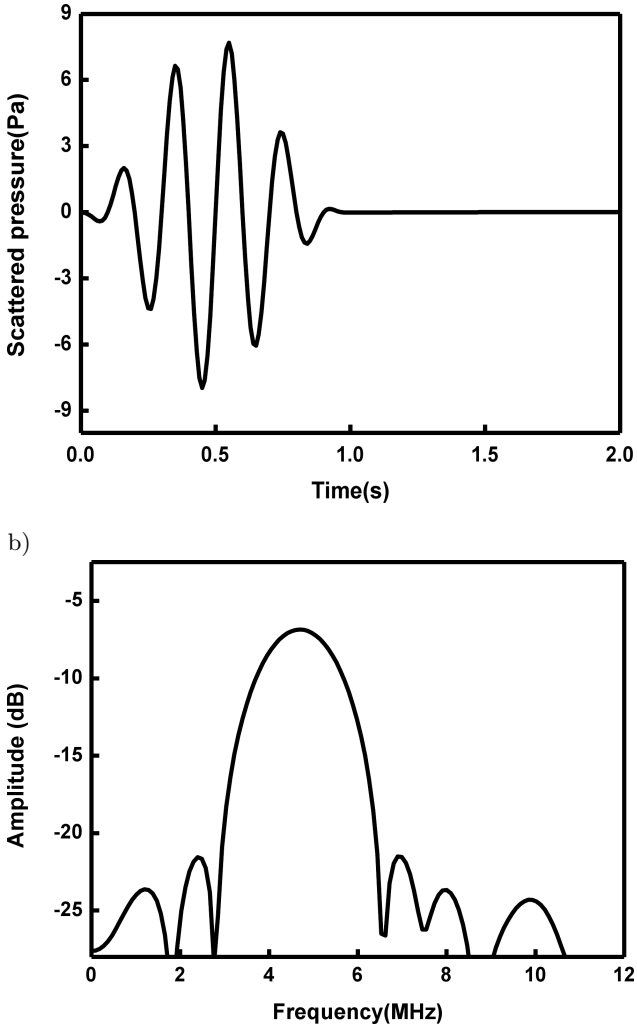

Fig. 8. Predicted scattered pressure wave for 4 μm air microbubbles in water from simulation obtained radial dynamics: a) scatter pressure response, b) the power spectrum. A subharmonic response is visible at a frequency of 2.5 MHz and 7.5 MHz. Also, a second harmonic response is visible at a frequency 10 MHz.

Figure 7 shows an example of a bubble with a non-linear oscillation behaviour. The bubble has an initial bubble radius of 4 μm. The plot shows that the driving pulse amplitude decreases towards zero and the bubble will continue to oscillate freely with lower amplitude. To estimate the spectral response for microbubble radius, the Fourier transform of pressure-time response was calculated (Fig. 8). In the acoustic response of the microbubble presented in Fig. 8 we can identify two different harmonics, $(1/2)f$, and $2f$ where f is the resonance frequency, which are clearly demonstrating the strong non-linear character of the microbubble response. To estimate the pressure-time response for packet of microbubbles, the Fourier transform of pressure time response was carried out by multiplying the transfer functions for each microbubble in the frequency domain. The resulting pressure response was then converted back into the discrete time domain by inverse Fourier transformation (Fig. 9). It is clear from this figure that the three harmonics $(1/2)f$, $(3/2)f$, $2f$ appear as shown in Fig. 8 but the bandwidths of harmonics are more wider than that shown in Fig. 8. Figure 9 shows scattering frequency responses for the four different number of microbubbles package. This figure demonstrates that the amplitude spectra for subharmonic and second harmonic increases with increasing the number of bubbles in the packet. Figure 10 shows the normalized scattering frequency responses for second harmonics of Fig. 9. It clearly presents that the one, two, four and five bubbles package yield 3 dB bandwidths of 7.36, 13.8, 16.56 and 23.92% of the center frequency respectively. These four curves have been scaled to the same peak value so as to emphasize the effect on bandwidth. Additionally, Fig. 11 shows the normalized scattering frequency responses for subharmonics at 2.5 MHz. From this figure it can be seen

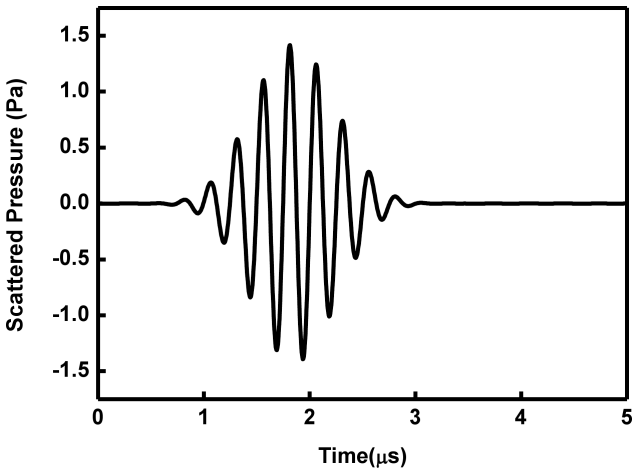

b)

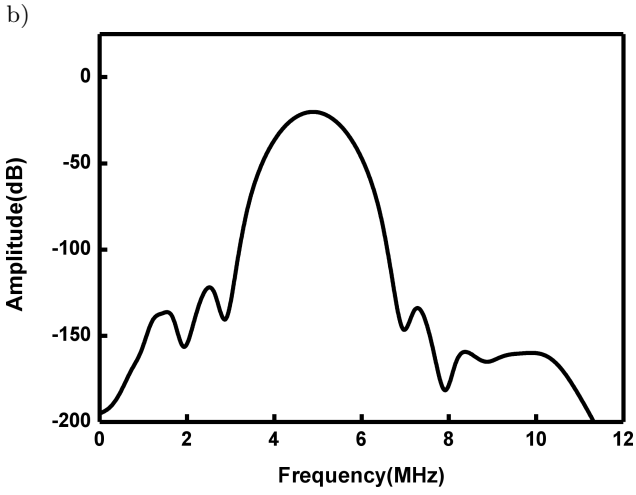

Four bubbles 3, 4, 5, 6

Fig. 9. Predicted scattered pressure wave for a package of air microbubbles with radius 3, 4, 5, and 6 μm in water from simulation obtained radial dynamics: a) scatter pressure response, b) the power spectrum. A subharmonic response is visible at a frequency of 2.5 MHz and 7.5 MHz. Also, a second harmonic response is visible at a frequency 10 MH.

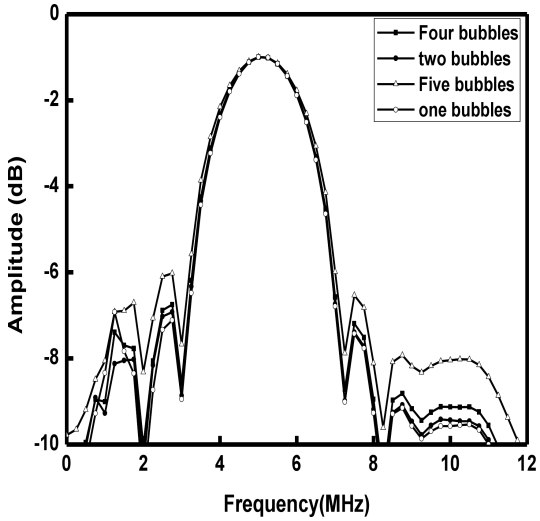

Fig. 10. Amplitude spectrum of scattered pressure for different number of air microbubbles normalized relative to the first harmonic.

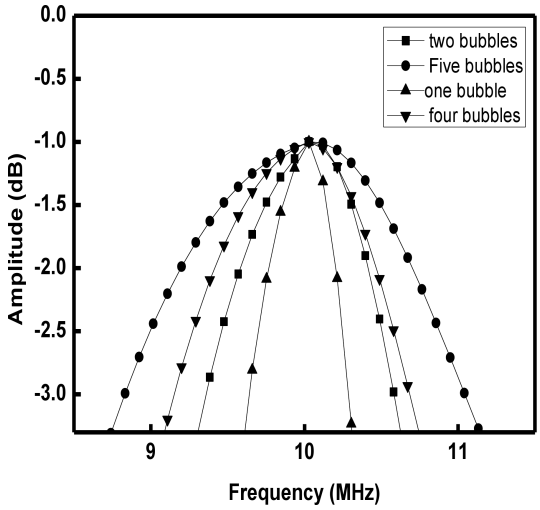

Fig. 11. Amplitude spectrum of second harmonic for different number of air microbubbles normalized to the same peak amplitude.

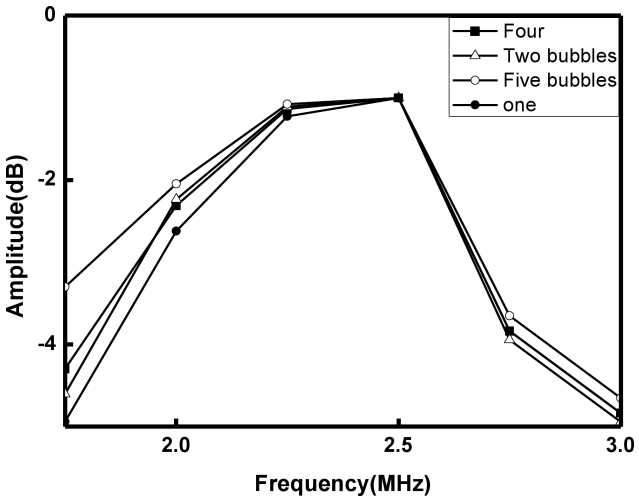

Fig. 12. Amplitude spectrum of subharmonic at 2.5 MHz for different number of air microbubbles normalized to the same peak amplitude.

that the one, two, four and five bubbles package yield −3 dB bandwidths of 30, 33, 35, and 40% of the center frequency respectively.

6. Conclusion

This paper has described a simulation of the signal pathway in a pulse echo system. The model included the piezoelectric transducer and different number of air microbubbles package in water. The simulation has been used to predict acoustic emission from radial dynamic of oscillating microbubbles package. Small amplitude behaviour and the higher-harmonic response were shown to be characterized more sensitively by the number of microbubble package. The acoustic response of targeted microbubbles was examined to improve nonlinear imaging techniques and aid signal quantification.

References

1. Ali M.G.S. (2000), *Analysis of Broadband Piezoelectric Transducers by Discreet Time Model*, Egypt. J. Sol., **23**, 287–295.
2. Ali M.G. (1999), *Discrete time model of acoustic waves transmitted through layer*, Journal of Sound and Vibration, **224**, 349–357.
3. Feng Z.C., Leal L.G. (1997), *Nonlinear bubble dynamics*, Ann. Rev. Fluid Mech., **29**, 201–243.
4. Leighton T.G. (1994), *The Acoustic Bubble*, Academic Press, London, UK.
5. Liang J.F., Chen W.Z., Shao W.H., Shui B. (2012), *A spherical Oscillation of Two Interacting Bubbles in an Ultrasound Field*, Chin. Phys. Lett., **29**.
6. Marmottant P., van der Meer S.M., Emmer M., Versluis M., Jong N., Hilgenfeldt S., Lohse D. (2005), *A model for large amplitude oscillations of coated bubbles accounting for buckling and rupture*, J. Acoust. Soc. Am., **118**, 3499–3505.
7. Neppiras E., Noltingk B. (1951), *Cavitation produced by ultrasonics: Theoretical conditions for the onset of cavitation*, Proceedings of the Physical Society Section B, **64**, 1032–1038.
8. Noltingk B., Neppiras E. (1950), *Cavitation produced by ultrasonics*, Proceedings of the Physical Society Section B, **63**, 674–685.
9. Plesset M. (1949), *The dynamics of cavitation bubbles*, Journal of Applied Mechanics, **16**, 277–282.
10. Poritsky H. (1952), *The collapse or growth of a spherical bubble or cavity in a viscous fluid*, pp. 813–821, Proceedings of the first US National Congress on Applied Mechanics.
11. Prosperetti A. (1984), *Bubble phenomena in sound fields*, Ultrasonic, **22**, 115–124.
12. Rayleigh L. (1917), *On the pressure developed in a liquid during the collapse of a spherical cavity*, Philosophical Magazine, **34**, 94–98.
13. Sijl J., Overvelde M., Dollet B., Garbin V., Jong N., Lohse D., Versluis M. (2011a), *Compression-only' behavior: A second order nonlinear response of ultrasound contrast agent micro bubbles*, J. Acoust. Soc. Am., **129**, 1729–1739.
14. Sijl J., Hendrik J. V, Rozendal T., Jong N., Lohse D., Versluisa M. (2011b), *Combined optical and acoustical detection of single microbubble dynamics*, J. Acoust. Soc. Am., **130**, 3271-3281.
15. Sijl J., Dollet B., Overvelde M., Garbin V., Rozendal T., Jong N., Lohse D., Versluis M. (2010), *Subharmonic behavior of phospholipid-coated microbubbles*, J. Acoust. Soc. Am., **128**, 3239–3252.
16. Vokurka K. (1985), *On rayleigh's model of a freely oscillating bubble*, I. Basic relations Czechoslovak J. Phys., **35**, 28–40.